Research Article

Cancer Immunology Research

Late-Stage Tumor Regression after PD-L1 Blockade Plus a Concurrent OX40 Agonist

Fanny Polesso[1], Andrew D. Weinberg[2], and Amy E. Moran[1]

Abstract

The protective capability of tumor antigen–specific T cells is regulated by costimulatory and inhibitory signals. Current approaches in cancer immunotherapy seek to restore the function of unresponsive T cells by blocking inhibitory pathways. In contrast, providing exogenous costimulatory signals to T cells also enhances antitumor functionality. By combining these two clinical approaches, we demonstrate the synergy of targeting PD-L1 together with the costimulatory molecule OX40, to enhance antitumor immunity. Concurrently blocking PD-L1 and providing a costimulatory agonist to OX40 increased the presence and functionality of tumor antigen–specific $CD8^+$ T cells with simultaneous enhancement of T-helper type 1 (Th1)-skewed $CD4^+$ T cells. This shift was functionally supported by increased glucose metabolism of antigen-specific $CD8^+$ T cells and the acquisition of granzyme B by regulatory T cells. Together, this mechanism promoted tumor regression of late-stage tumors beyond that achieved by either blockade as monotherapy. These findings indicate that targeting both T-cell intrinsic (OX40) and extrinsic (PD-L1) regulatory molecules increases the bioenergetic potential of T cells, thereby expanding functional and tumor antigen–specific T cells.

Introduction

The tumor necrosis receptor super family (TNFR) member OX40 is a costimulatory molecule induced following TCR engagement, much like PD-1. Within the tumor microenvironment, TCR signals are often devoid of costimulation (either via CD28/B7 or OX40/OX40L interactions), and the lack of costimulation renders T cells dysfunctional. When OX40 is ligated by either its natural ligand, OX40L, or via an agonist antibody, it can enhance T-cell proliferation, survival, effector cell function, restore function of anergic T cells, and promote tumor regression (1, 2). OX40 is expressed on both $CD4^+$ and $CD8^+$ T cells in the tumor, and the antitumor therapeutic benefit requires both of these T-cell subsets (3). In studies with parallel functional and transcriptional analyses evaluating the impact of OX40 activation, it has been revealed that OX40 ligation increased regulators of T-cell metabolism in murine $CD4^+$ T cells (4). In support of this observation, others have reported that OX40 signaling increases the expression of interferon response factor 4 (Irf4) (5), a key metabolic regulator of T cells. Therefore, it is plausible that OX40 signaling metabolically reprograms T cells, thereby supporting their increased clonal expansion, effector function, and survival.

The PD-1/PD-L1 axis has been successfully targeted with inhibitory antibodies against PD-1 and PD-L1 and therapeutic responses have been observed with both. Although these proteins share a common pathway, it is appreciated that their expression is largely restricted to distinct cell populations. In the tumor microenvironment, PD-1 expression occurs predominantly on T cells and is upregulated during the effector phase of T-cell activation, similar to OX40, or with chronic TCR stimulation. PD-L1 (also referred to as B7-H1) is expressed on cells of the myeloid lineage including dendritic cells and macrophages (6) and its expression can be induced on lymphoid, endothelial, and epithelial lineages as well as tumor cells upon exposure to IFNγ and TNFα (7). PD-1 signaling inhibits T-cell activation by suppressing signaling from the costimulatory molecule CD28 (8), whereas PD-L1 signaling in tumor cells was shown to promote mTOR signaling and support glycolytic metabolism (9). Therefore, despite PD-1 and PD-L1 sharing an inhibitory axis, monoclonal antibodies targeting these individual proteins may have different therapeutic outcomes when targeted alone or in combination with other therapies. One possible mechanism of synergy was suggested in studies by Chang and colleagues, which revealed that tumor cell metabolism could be directly regulated by anti–PD-L1 (9). These data proposed that PD-L1 blockade may enhance T-cell function through the increase of free glucose within the tumor microenvironment, leading to a metabolically favorable microenvironment for tumor antigen–specific T cells.

Two papers suggest that PD-1 blockade in combination with OX40 agonists attenuates the therapeutic benefit of OX40 immunotherapy as a single agent. Shrimali and colleagues report that antigen-specific $CD8^+$ T cells coexpress PD-1 and OX40 after stimulation. Despite increased proliferation and IFNγ production after anti–PD-1/anti-OX40 treatment, they underwent higher rates of apoptosis (10). In support of this finding, Messenheimer and colleagues also report that, despite an increase in proliferation

[1]Department of Cell, Developmental and Cancer Biology, Knight Cancer Institute, Oregon Health and Science University, Portland, Oregon. [2]Earle A. Chiles Research Institute, Robert W. Franz Cancer Research Center, Providence Portland Medical Center, Portland, Oregon.

Note: Supplementary data for this article are available at Cancer Immunology Research Online (http://cancerimmunolres.aacrjournals.org/).

A.D. Weinberg and A.E. Moran share senior authorship of this article.

Corresponding Author: Amy E. Moran, Oregon Health and Science University, 3181 SW Sam Jackson Park Road, KCRB-CDCB, Portland, OR 97239-3098. Phone: 503-494-9711; Fax: 503-494-4253; E-mail: moranam@ohsu.edu

doi: 10.1158/2326-6066.CIR-18-0222

of $CD8^+$ T cells after anti–PD-1/anti-OX40 treatment, there was a total decrease in $CD8^+$ tumor-infiltrating lymphocytes (11, 12) and a lack of therapeutic benefit when these antibodies are concurrently administered.

In this study, we tested the hypothesis that in mice bearing late-stage tumors, concurrent targeting of PD-L1 (blockade) would enhance OX40 (agonist) immunotherapy and thereby promote long-term tumor-free survival. We uncover mechanisms of synergy between anti–PD-L1 + anti-OX40 and reveal that antigen-specific $CD8^+$ T cells exposed to combination therapy take up more glucose than single-agent–treated animals, have increased bioenergetic potential at baseline and upon antigen receptor ligation. We report improved survival outcomes in mice treated with concurrent anti–PD-L1 + anti-OX40 combination therapy and large, late-stage tumor regression.

Materials and Methods

Animals, tumor models, and antibodies

Nur77GFP mice were provided by K.A. Hogquist (University of Minnesota, Minneapolis, MN), maintained as heterozygous transgene carriers and bred to either C57Bl/6 (B6) or 129 mice purchased from the Jackson Laboratory. C57BL6 FoxP3-RFP mice were purchased from the Jackson Laboratory and maintained as homozygous transgene carriers. All animals were bred and maintained under specific pathogen-free conditions in the Providence Portland Medical Center (PPMC; Portland, OR) or Oregon Health and Science University (OHSU) animal facility. Males and females were used for the 3′-methylcholanthrene (MCA) 205 studies presented; only males were used for d42m1–T3 studies. For survival experiments, WT female B6 and BALB/c mice were purchased from the Jackson Laboratory. All animal experimentation was approved by and performed according to the guidelines from the Institutional Animals Care and Use Committee at PPMC and/or OHSU. Murine MCA205 sarcoma cells (gift of Suyu Shu) and CT26 colon carcinoma cells (gift of Hy Levitsky) were propagated *in vitro* using complete media, RPMI-1640 (Lonza) containing 0.292 ng/mL glutamine, 100 U/mL streptomycin, and penicillin, 1× nonessential amino acids, 1 mmol/L sodium pyruvate, and 10 mmol/L HEPES (Sigma-Aldrich). d42m1-T3 cells were generously provided by Robert Schreiber (Washington University School of Medicine, St. Louis, MO) and cultured in the above culture media supplemented with 0.1% 2-mercaptoethanol. All cell lines were tested in September 2017 after obtaining them from A. Weinberg (Earle A. Chiles Research Institute) and confirmed to be *Mycoplasma* and endotoxin-free using the MycoAlert Detection kit (Lonza) and the Endosafe-PTS system (Charles River Laboratories). Tumor cells were passaged no more than 3 passages after thawing before being used *in vivo*. Cells were not authenticated prior to performing these studies. All culture media reagents were purchased from Hyclone Laboratories unless noted otherwise. Control rat IgG was purchased from Sigma-Aldrich. OX40 (OX86) mAb was produced in the laboratory from a hybridoma and affinity purified over protein G columns. Programmed death ligand-1 (PD-L1; clone 10F.9G2) purified mAb was purchased from Bio X Cell. Animals were randomly assigned to treatment cohorts, and tumors were ∼50 to 70 mm^2 (by two-dimension caliper measurement) at the start of treatment. Any animal with a tumor >200 mm^2 was euthanized per our guidelines from the Institutional Animal Care and Use Committee. No outliers were excluded from the data presented.

Lymphocyte isolation and analysis

Tumor-draining lymph node (dLN; inguinal) and spleens were harvested and processed to obtain single-cell suspensions using frosted ends of microscope slides. Spleens were incubated with ammonium chloride potassium lysing buffer (Lonza) for 3 minutes at room temperature to lyse red blood cells. Cells were rinsed with PBS containing 1% FBS and 4 mmol/L EDTA. For flow cytometry analysis, cells were incubated for 20 minutes on ice with zombie yellow fixable viability dye, TCRβ (H57-597), CD4 (RM4-5), CD8 (53-6.7), PD1 (J43), PD-L1 (MIH5), B220 (RA3-6B2), CD11c (HL3), CD44 (IM7), CD25 (PC61.5), CD62L (MEL014), KLRG1 (2F1), Ki67 (SolA15), and Thy1.1 (HIS51). All antibodies and viability dies were purchased from eBioscience, BioLegend, or BD Biosciences. MHC class I tetramers were generated by the National Institute of Health Tetramer Facility for assessing H-$2K^b$:mLama4 (VGFNFRTL) and H-$2K^b$:mAlg8 (ITYTWTRL) in d42m1-T3 tumors and H-$2K^b$:OVAp (SIINFEKL) tetramer for evaluating ovalbumin-specific responses. Unless noted otherwise in the figure legend, cells were gated through live/$TCR\beta^+$ gates for analysis. Intracellular proteins FoxP3, Tbet, Ki67, IFNγ, TNFα, IL2, and granzyme B were detected using the FoxP3 Transcription Factor Concentrate and Diluent from eBioscience. Fluorescence-minus-one controls were used to determine positive fluorochrome signals. Cells were analyzed with an LSR II or Fortessa flow cytometer (BD Biosciences) using FlowJo software (Tree Star). T-cell sorts were performed on an Aria (BD Biosciences) with a 70-μm nozzle.

Metabolism assays

Tumors were digested according to our standard protocol. Cells (3.5×10^6) from tumor preparations were pulsed with 0.64 μmol/μL 2NBDG (Invitrogen) in glucose-free RPMI for 30 minutes at 37°C. Cells were then surfaced stained on ice. A "cold" control (incubation on ice) was performed in parallel for background control. For Seahorse assays, 1.2×10^5 purified T cells/well were plated on poly-d-lysine coated Seahorse culture plates in minimal assay media (unbuffered DMEM pH 7.4, 25 mmol/L glucose, 2 mmol/L L-glutamine, 1 mmol/L sodium pyruvate) and analyzed using a Seahorse XFe96 (Agilent). Basal ECAR (extracellular acidification rates) and OCR (oxygen consumption rates) were taken for 30 minutes. In some experiments, one drug delivery chamber of the Seahorse analyzer was loaded with PMA/ionomycin (Cell Stimulation Cocktail, eBioscience), and cells were stimulated and mitochondrial response was measured after measuring basal respiration. After PMA/ionomycin stimulation, ECAR/OCR readings were taken for another 60 minutes.

Tumor challenge and tumor immune infiltration

For survival experiments, 0.4×10^6 MCA205 or CT26 tumor cells were injected s.c. into the right flank of B6 or BALB/c mice, respectively. When the tumor reached ∼50 to 70 mm^2 (days 10–12 after tumor inoculation), the mice were treated with 2 doses of 250 μg rat IgG or anti-OX40 4 days apart, and/or 4 doses of 200 μg anti–PD-L1 3 days apart (10 mice per treatment group). Tumors were measured 3 times per week with microcalipers, and animals were euthanized when the tumors reached 150 mm^2. For phenotyping experiments, 0.5×10^6 MCA205 or 1×10^6 d42m1-T3 tumor cells were injected on both hind flanks of B6, 129, or Nur77GFP; 129 F1 mice,

respectively (minimum of 3 animals per group per experiments). When the tumors reached ~70 mm^2, the tumor-bearing mice were treated with 2 doses of 250 μg rat IgG or anti-OX40 4 days apart, and/or 3 doses of 200 μg anti–PD-L1 3 days apart. All antibody injections were given i.p. TILs were harvested by dissection of tumor tissue into small fragments in a 50-cc conical tube followed by digestion at room temperature in a bacterial shaker at 180 rpm for 30 minutes in 1 mg/mL collagenase type IV (Worthington Biochemicals), 100 μg/mL hyaluronidase (Sigma-Aldrich), and 20 mg/mL DNAse (Roche) in PBS. Following filtration and further cell disruption with a 1-cc syringe plunger through a 70-μm nylon cell strainer (BD Biosciences), tumor cells, splenocytes, and lymphocytes were stained.

In vitro activation, intracellular cytokine staining, regulatory T cell (Treg) suppression assay

Splenocytes and bulk TILs were plated at 10^6 cell/well in 96-well plates and stimulated for 4 to 5 hours with anti-CD3 (145-2C11) or PMA (80 nmol/L) and ionomycin (1.3 μmol/L) in the presence of brefeldin A (BFA). Cells were then stained for surface markers, fixed and permeabilized using either the BD Cytofix/CytoPerm or eBioscience Foxp3 kit, and stained for intracellular cytokines. $FoxP3^+$ Tregs were sorted from spleens and tumors of FoxP3-RFP animals treated with respective antibody therapy. In some cases, sorted Tregs were labeled with CFSE. Conventional $CD4^+$ T cells (Tconv) were isolated from spleens of Thy1.1 animals using CD4 isolation EasySep kits (Stemcell Biotechnology) with addition of anti-CD25-biotin antibody at 1:300 dilution to the antibody cocktail to deplete Tregs, and labeled with Cell Trace Violet (CTV). Varying ratios of $FoxP3^+$ sorted Tregs were cultured with CTV labeled $CD4^+$ Tconv (minimum number of Tconv: 30,000 cells per 96-well plate), in the presence of irradiated WT CD45.1 antigen-presenting cells (2× number of Tconv) and 0.5 mg/mL anti-CD3 for 3 days. Treg-suppressive function was measured by analyzing CTV dilution within the $CD4^+$ Tconv cell population.

TCR sequencing

TCR sequencing tumors from MCA205 tumor–bearing animals treated with rat IgG, anti-OX40, anti–PD-L1, or combination therapy (see treatment scheme and doses in tumor challenge and tumor immune infiltration—phenotyping) were harvested on the day after the third anti–PD-L1 treatment. TILs and splenocytes were enriched for $CD8^+$ T cells by using a negative selection mouse $CD8^+$ T-cell isolation kit (STEMCELL Technologies), stained and sorted for $CD8^+$GFPhi and $CD8^+$GFPlow cells using an Aria cell sorter (BD Biosciences). Genomic DNA was extracted using DNeasy blood and tissue kit (Qiagen). TCRβ chain sequencing was performed using the Mouse ImmunoSEQ kit from Adaptive Biotechnologies. Clonality is defined as the measure equal to the inverse of the normalized Shannon entropy of all productive clones in a sample (13). TCRb chain sequences are provided (Supplementary Table S1).

Infections

L. monocytogenes strain ActA-Lm-OVA was generously provided from Keith Bahjat. This strain secretes full-length chicken ovalbumin controlled by the *hly* promoter. Bacteria were grown to mid-log in brain–heart infusion (14) broth, washed in PBS, and 5×10^6 CFU was injected intravenously in B6 mice (3 animals per group) in 200 μL total volume. One day after infection, the animals were injected i.p. with 250 μg of rat IgG or anti-OX40 (2 doses, 4 days apart) and/or 200 μg anti–PD-L1 (3 doses, 3 days apart). The day after the third injections of anti–PD-L1, spleens were harvested and splenocytes isolated. $CD8^+$ T cells were enriched using a negative selection mouse $CD8^+$ T cells isolation kit (STEMCELL Technologies), stained, and naïve $CD8^+$ T cells (live, $CD8^+$, $CD44^{low}$, $CD62L^{hi}$, $CD69^-$) and OVA-specific $tetramer^+$ $CD8^+$ (live, $CD8^+$, $CD44^{hi}$, $CD62L^{low}$, $CD69^+$, $H\text{-}2K^b$:OVA^+) were sorted using an Aria cell sorter (BD Biosciences).

Statistical analysis

Statistical analysis was performed using unpaired two-tailed Student *t* test (for comparison between two groups), one-way ANOVA for multiple comparisons, or the Mantel–Cox method (log-rank test) for survival analysis using GraphPad Prism 6 (GraphPad Software). Error bars represent SEM unless noted otherwise in the figure legend. Statistical tests and *P* values are specified for each panel in the respective figure legends, and *P* values > 0.05 were considered significant. Biological replicates (individual animals) for each experiment are indicated in the figure legends.

Study approval

All animal experiments were approved by the Institutional Animal Care and Use Committee of Earle A. Chiles Research Institute at PPMC and OHSU Department of Comparative Medicine.

Results

OX40 agonist with PD-L1 blockade is curative in mice harboring large tumors

We have previously demonstrated that treatment of tumor-bearing animals with an OX40 monoclonal agonist antibody increases the frequency of IFNγ-producing T cells and delays tumor growth (1). However, even with a 2-fold increase in this T-cell population, the animals still succumbed to their tumor burden (1). Therefore, using Nur77GFP mice to identify tumor-associated antigen-specific T cells, we asked if other actionable pathways enhance antitumor T-cell function. Animals were treated with agonist OX40 (anti-OX40) according to the treatment schedule (Fig. 1A), and we observed a >2-fold increase in frequency of $CD8^+PD\text{-}1^+Nur77GFP^{hi}$ T cells (Fig. 1B and C) and significantly increased PD-L1 expression on $B220^+$ and $CD11c^+$ populations within the tumor (Fig. 1D) and to a lesser extent in the spleen (Fig. 1E). Taken together, this suggested that despite OX40 agonists expanding T cells encountering high-affinity tumor-associated antigens within the tumor, PD-1/PD-L1 is one mechanism limiting their function.

We hypothesized that simultaneously targeting OX40 and blocking PD-L1 would enhance antitumor immunity. Therefore, we established a treatment schedule based on previously published therapeutic regimes (Fig. 1A; ref. 15). In these experiments, we waited for the tumors to reach 50 to 75 mm^2, a size at which agonist OX40 or PD-L1 blockade alone has minimal therapeutic efficacy (1).

In sarcoma and adenocarcinoma (Supplementary Fig. S1) models, anti-OX40 + anti–PD-L1 was curative in 30% to 60% of mice treated (Fig. 1F). When compared with the control

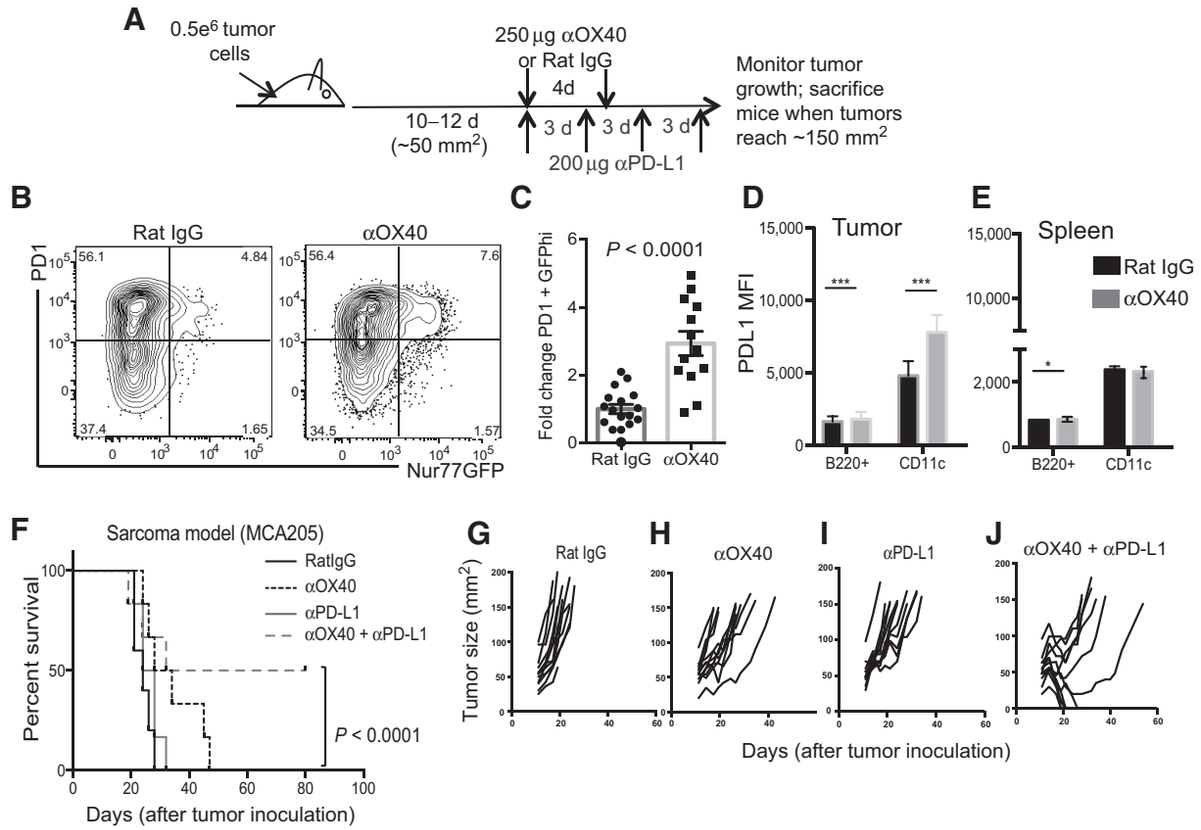

Figure 1.

OX40 agonists synergize with anti–PD-L1 to promote tumor regression. **A,** Experimental design for survival experiments. Tumors were measured 3 times per week, and animals were euthanized when the tumors were >150 mm^2. **B,** Representative flow cytogram and percentages of total $CD8^+$ T cells isolated from the sarcoma model MCA205 after anti-OX40 treatment alone. **C,** Fold change in percentages of $PD1^+Nur77GFP^{hi}$ $CD8^+$ T cells. PD-L1 MFI in the tumor (**D**) and spleen (**E**). **F,** Survival of MCA205-bearing C57Bl/6 mice following immunotherapy. Tumor growth curves of MCA205-bearing C57Bl/6 mice treated with (**G**) rat IgG (**H**) anti-OX40, (**I**) anti–PD-L1, or (**J**) anti-OX40 + anti–PD-L1. **B–E,** Data combined from at least 3 independent experiments with $n = 3$ animals per treatment group per experiment. Unpaired two-tailed Student t test was used for statistical analysis. *, $P < 0.05$; **, $P < 0.01$; ***, $P < 0.001$. **F–J,** Data are representative of more than 3 independent experiments with 5–10 animals per treatment group/experiment. **F,** Unpaired two-tailed Student t test was used for statistical analysis.

(Fig. 1G), neither anti-OX40 (Fig. 1H) nor anti–PD-L1 (Fig. 1I) mediated long-term survival in these tumor models as single therapies. However, we observed rapid tumor regression in animals receiving anti-OX40 + anti–PD-L1 combination therapy (Fig. 1J). These mice remained tumor-free for more than 40 to 60 days and were protected from tumor rechallenge (Supplementary Fig. S2).

Combination therapy drives the expansion of $CD8^+$ T cells receiving strong TCR signals

To understand the synergy between anti-OX40 and PD-L1 blockade, we bled tumor-bearing animals after the third dose of anti–PD-L1, a time point at which we observed tumor regression (Fig. 1J). Anti-OX40 or anti–PD-L1 as single therapy modestly increased the frequency of antigen-experienced $CD8^+$ T cells in the periphery, and there was a 3- to 4-fold increase in frequency of $CD8^+CD44^{hi}$ T cells in the periphery of combination therapy–treated animals (Fig. 2A). Dominant tumor antigens in the MCA205 tumor model have not been defined; therefore, we used Nur77GFP mice to identify $CD8^+$ T cells that recently encountered cognate antigen *in situ*. Briefly, GFP is under the control of the nuclear orphan receptor Nur77 and is sensitively regulated by T-cell receptor signal strength (16). Using this model system, we reported that tumor antigen–reactive T cells in the tumor dLNs can be identified independently of knowing the tumor antigen (1). Thus, we evaluated the frequency of $CD8^+$ T cells receiving strong TCR signals ($Nur77GFP^{hi}$) in the dLNs (Fig. 2B and C) of Nur77GFP animals the day after the third dose of anti–PD-L1. This combination therapy increased the frequency of $CD8^+Nur77GFP^{hi}$ T cells >3-fold, whereas single-agent therapy with either OX40 agonist or PD-L1 blockade increased this population 1.5- to 2-fold (Fig. 2C). Moreover, we observed a significant increase in the frequency (Fig. 2D) and total number (Fig. 2E) of $CD8^+PD1^+CD25^{hi}$ T cells in these animals. This expansion can be accounted for in part by a systemic increase in proliferation (as measured by Ki67) of $CD8^+$ T cells (Fig. 2F). Within the tumor, we observed a significant increase in the proliferation of T cells receiving strong TCR signals as measured by Nur77GFP expression (Fig. 2G and H). The majority of

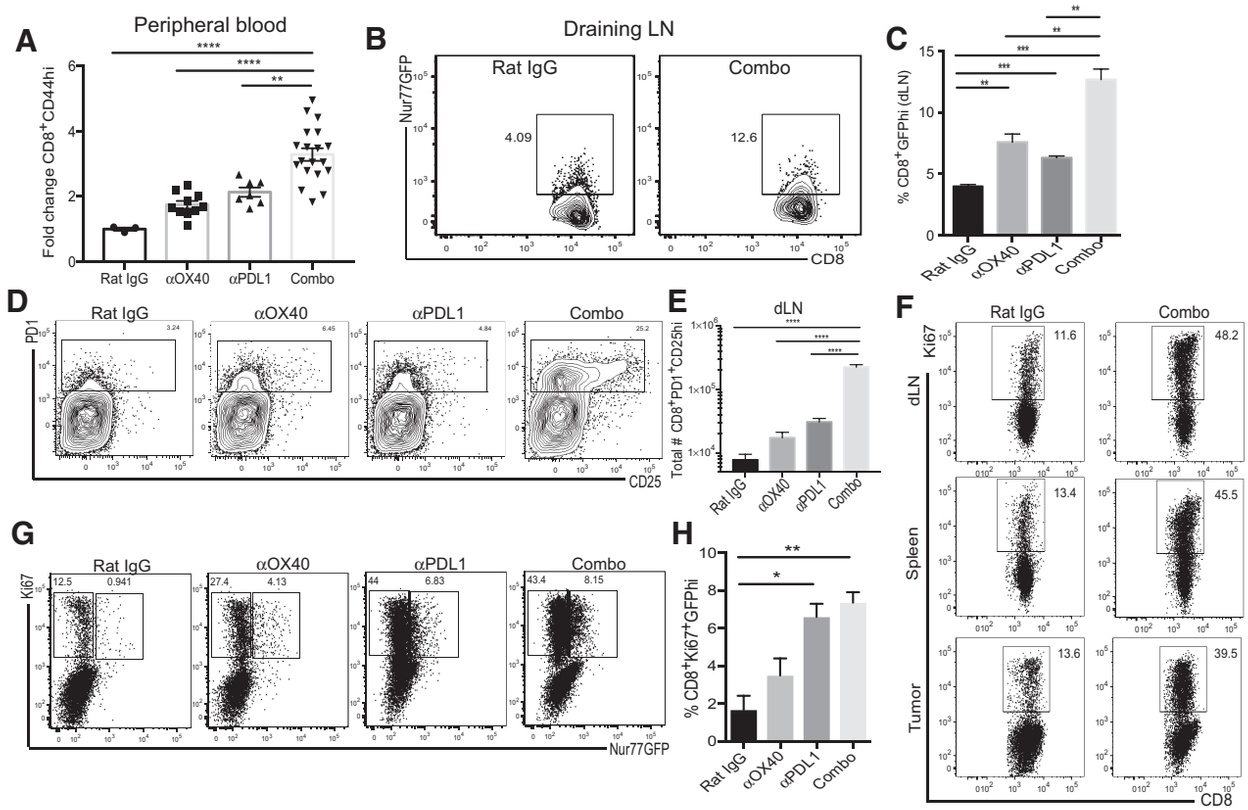

Figure 2.

Combination therapy expands T cells receiving strong TCR signals. Nur77GFP animals were inoculated with MCA205 tumors on both flanks and treated according to the experimental design (Fig. 1A). The day after the third anti–PD-L1 treatment, mice were (**A**) bled or (**B**) euthanized, and tumor dLNs were isolated. **C,** Frequency of Nur77GFP$^+$ CD8$^+$ T cells in the dLNs after combination therapy. **D,** Frequency and (**E**) total number of CD8$^+$PD1$^+$CD25^{hi} cells in the tumor dLNs. **F,** Frequency of Ki67$^+$CD8$^+$ T cells in the tumor dLNs, spleen, and tumor. **G,** Representative flow cytogram and (**H**) summary of Ki67$^+$Nur77GFP^{hi} CD8$^+$ T cells in the tumor of treated animals. Data are representative of at least 3 independent experiments with $n = 3$ animals per treatment group per experiment. Unpaired Student t test was used for statistical analysis. *, $P < 0.05$; **, $P < 0.01$; ***, $P < 0.001$; ****, $P < 0.0001$.

proliferating CD8$^+$ T cells in the tumor were GFP^{low}, suggesting antigen-independent bystander proliferation, loss of GFP expression due to proliferation, and/or the expansion of lower-affinity CD8$^+$ T-cell clones.

Tumor antigen–specific CD8$^+$ T-cell numbers and function increased after combination therapy

Given the increase in CD8$^+$ T cells receiving high-affinity TCR signals in tumor and dLNs, we asked if combination therapy increased the differentiation of tumor antigen–specific CD8$^+$ T cells. To address this question, we used a tumor model with defined endogenous mutated tumor-rejection antigens trackable with MHC tetramer reagents to interrogate the tumor antigen–specific CD8$^+$ T-cell response after single-agent or combination therapy.

We observed >10-fold increase over the rat IgG control in the frequency (Fig. 3A) and total number (Fig. 3B) of CD44^{hi} mAlg8-specific CD8$^+$ T cells in the tumor dLNs of combination therapy–treated animals. Tumor antigen–specific T cells were enriched for KLRG1 expression and downregulated the integrin CD62L (Fig. 3C), markers of effector memory differentiation. In the dLNs, there was approximately a 10-fold increase in the total number of effector memory T cells (ref. 17; defined as KLRG1$^+$CD62L^{low}) after combination therapy (Fig. 3D). Similarly, we observed an increase in the frequency (Fig. 3E) and total number (Fig. 3F) of effector memory mAlg8-specific CD8$^+$ T cells with a concurrent decrease of central memory CD8$^+$ T cells (KLRG1^{low}CD62L^{hi}; Fig. 3E) in the tumor of combination therapy–treated animals. The greatest difference in the tumor was observed between the untreated animals and the combination therapy animals (Fig. 3F).

Moreover, the function of tumor antigen–specific CD8$^+$ T cells was altered after combination therapy. We observed an increase in the frequency of cytokine-producing cells in the tumor dLNs (Fig. 3G) and tumor (Fig. 3H) of combination-treated animals when compared with either single agent alone, a finding consistent with enhanced T_{EM} differentiation. Moreover, there was a significant increase in the total number of CD8$^+$ T cells producing TNFα (Fig. 3I), IFNγ (Fig. 3J), or both cytokines (Fig. 3K). Granzyme B production by bulk tumor-infiltrating (Fig. 3L) and tumor antigen–specific CD8$^+$ T cells (Fig. 3M) was significantly increased with individual immunotherapies, yet combination therapy led to a 10-fold increase in CD8$^+$ T cells producing this lytic (Fig. 3N). The antitumor effect of the combination therapy was dependent on these CD8$^+$ T cells (Supplementary Fig. S3).

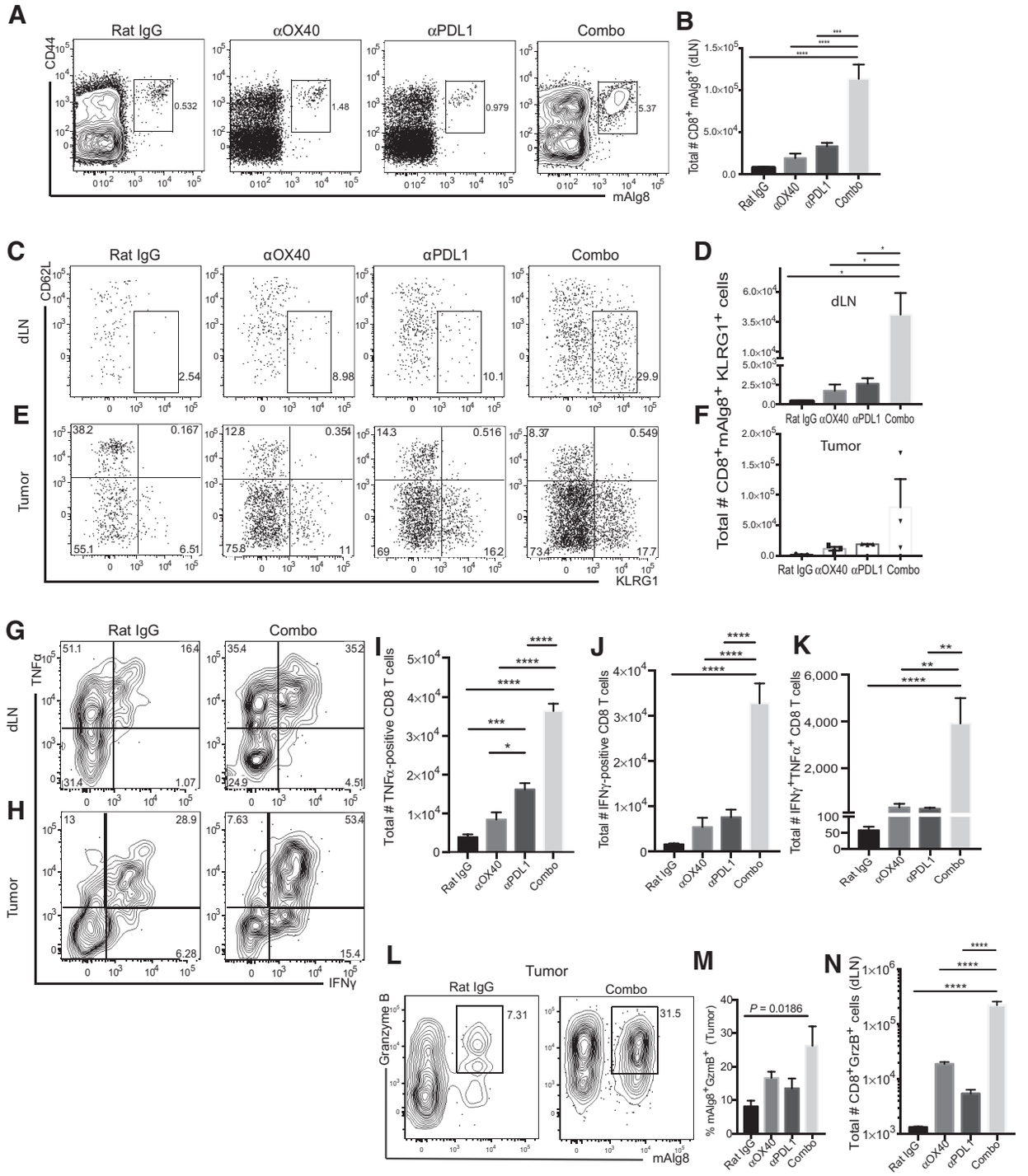

Figure 3.

Increase of functional tumor antigen–specific CD8$^+$ T cells. Animals were inoculated with 1×10^6 d42m1-T3 tumor cells in the hind flank. Approximately day 12 after inoculation, animals were treated as in Fig. 1A. **A,** Frequency and (**B**) number of CD44^{hi} mAlg8$^+$ CD8$^+$ T cells in the tumor dLNs. **C–F,** Frequency and total number of CD62L^{low} and KLRG1^{hi} CD8$^+$mAlg8$^+$ T cells from the dLNs (**C–D**) and tumor (**E–F**). Cytogram of cytokine expression after PMA/ionomycin stimulation for 4 hours of (**G**) bulk lymphocytes or (**H**) digested tumor preparations. Total number of (**I**) TNFα$^+$, (**J**) IFNγ$^+$, and (**K**) TNFα$^+$IFNγ$^+$ CD8$^+$ T cells in the tumor dLNs. **L,** Representative flow cytogram and (**M**) frequency of CD8$^+$mAlg8$^+$GrzmB$^+$ T cells. **N,** Total number of CD8$^+$GrzmB$^+$ T cells in the tumor. Data are combined from 2 to 4 independent experiments. Unpaired Student *t* test or one-way ANOVA for multiple comparisons was used for statistical analysis. *, $P < 0.05$; **, $P < 0.01$; ***, $P < 0.001$; ****, $P < 0.0001$.

Combination therapy enhances clonal expansion of CD8$^+$ TILs

In a model of adoptive cell therapy, tumor antigen–specific CD8$^+$ T cells were observed to be dysfunctional at controlling tumor growth after an initial period of cytotoxic function. These T cells also lost the ability to upregulate the NFAT-regulated gene, Nur77, despite antigen presence in the tumor (1). Agonist OX40 immunotherapy restored NFAT-mediated Nur77 induction, and this therapy rescued failed adoptive cell therapy (1). Given these observations together with the increase in the proliferation of CD8$^+$ T cells receiving strong TCR signals after combination therapy (Fig. 2F–H), we hypothesized that combination therapy may expand CD8$^+$ T cells receiving strong TCR signals *in situ*.

Nur77GFP was used to detect T cells receiving strong TCR signals. Tumor-bearing animals were treated with single or combination therapy. OX40 agonists increased the proliferation and frequency of tumor-infiltrating CD8$^+$ T cells receiving strong TCR signals, an observation that we did not see with anti–PD-L1 single therapy (Fig. 4A). Periodically, an animal would have a significant increase in CD8$^+$Nur77GFP^{hi} T cells after combination therapy, but this was not a uniform observation in all animals (Fig. 4A and Fig. 2H). Because these were terminal studies, animals were euthanized at the time of tumor resection, thereby limiting our ability to correlate whether the significant increase in CD8$^+$Nur77GFP^{hi} TIL corresponded with tumor rejection. Despite this challenge, these data suggested that the expansion of CD8$^+$ T cells receiving strong TCR signals was driven by both an OX40 agonist and PD-L1 blockade.

To understand if the efficacy of the combination therapy was the expansion of T cells with lower-affinity TCRs, a question that we could not address with the Nur77GFP model, we sorted CD8$^+$Nur77GFP^{hi} and GFP^{low} T cells from the tumor of individual mice (Fig. 4B), isolated genomic DNA, and sequenced the TCRβ chains from each group. Using the ImmunoSeq platform, we could assess the clonality of the T-cell response. All therapies enhanced the clonality of CD8$^+$ tumor-infiltrating T-cell clones (Fig. 4C and D), some of which were receiving high-affinity signals (Fig. 4E, gray squares). It was noticeable that the top tumor-infiltrating T-cell clones all increased in frequency after OX40 immunotherapy (whether Nur77GFP^{hi} or ^{low}) but not with anti–PD-L1 alone. A few abundant tumor-infiltrating CD8$^+$ T-cell clones could be detected after anti–PD-L1 therapy, yet many of the remaining top clones were at frequencies below 1.5% (Fig. 4E; compare gray/black frequencies). CD8$^+$ T cells were required for the therapeutic efficacy of the combination therapy as tumor-bearing animals depleted of CD8$^+$ T cells prior to treatment succumbed to their disease (Supplementary Fig. S3). Therefore, it appears that agonist OX40 immunotherapy enhances clonal expansion of tumor-infiltrating CD8$^+$ T cells, some of which are actively encountering their cognate antigen. This suggests that CD8$^+$ T-cell clonal expansion alone is inadequate to mediate tumor rejection of an established tumor, and anti–PD-L1 therapy enhances the tumor microenvironment and/or function of these expanded clones.

Combination therapy increases a Th1-skewed CD4$^+$ T-cell response

Given that OX40 agonists increase CD4$^+$ T-cell function, we analyzed the CD4$^+$ T-cell compartment in single versus combination therapy–treated tumor-bearing animals after combination therapy (Fig. 1A). Treating animals with OX40 agonist and PD-L1 blockade significantly increased the frequency (Fig. 5A and B) and total number (Fig. 5C) of Tconv and Tregs in the tumor dLNs, an increase that was significantly greater than either single therapy agent alone.

OX40 agonists enhance IL12R expression and IL12 promotes T-helper type 1 (Th1) CD4$^+$T-cell differentiation and we observed that combination therapy promoted the expansion (Fig. 5D and E) and differentiation (Fig. 5F and G) of a population of Tbet$^+$ CD4$^+$ T cells in the tumor dLNs, prompting us to assess Th1 cytokine production. We noted an increase in cytokine-producing CD4$^+$ T cells in the tumor (Fig. 5H) after *ex vivo* stimulation and a 3-fold increase over the rat control in the frequency of polyfunctional (T cells making multiple cytokine) CD4$^+$ T cells in the tumor of combination therapy–treated animals (Fig. 5I). When

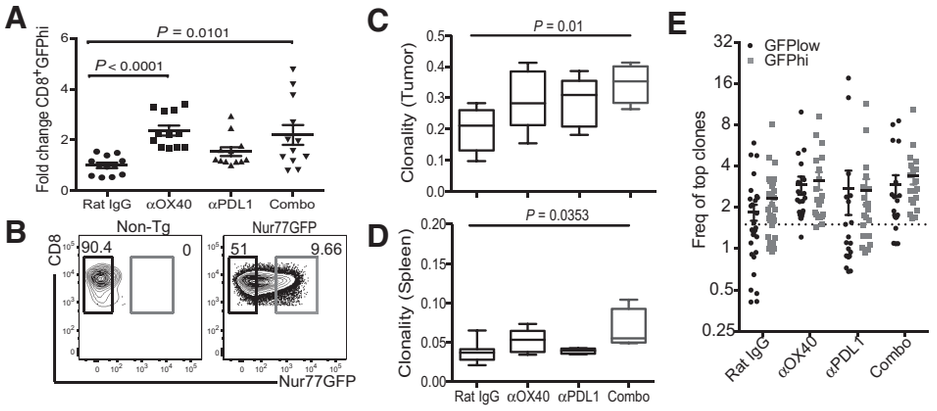

Figure 4.

Combination therapy enhances CD8$^+$ T-cell clonal expansion. Nur77GFP animals were inoculated with MCA205 tumors and treated according to Fig. 1A with single-agent or combination therapy prior to harvesting TIL. **A,** Fold change of CD8$^+$Nur77GFP^{hi} TIL (compared with rat IgG) in the tumor. **B,** Representative sort gates and clonality index from pooled CD8$^+$GFP^{hi} and GFPlow (**C**)TIL or (**D**) splenic CD8$^+$ T cells that underwent TCRβ sequencing performed on genomic DNA. **E,** Total abundance of the top CD8$^+$ T-cell clones (top 10 clones combined from multiple animals) of all clones sequenced from the tumor. Data are combined from 2 to 3 animals per treatment from at least 2 independent experiments.

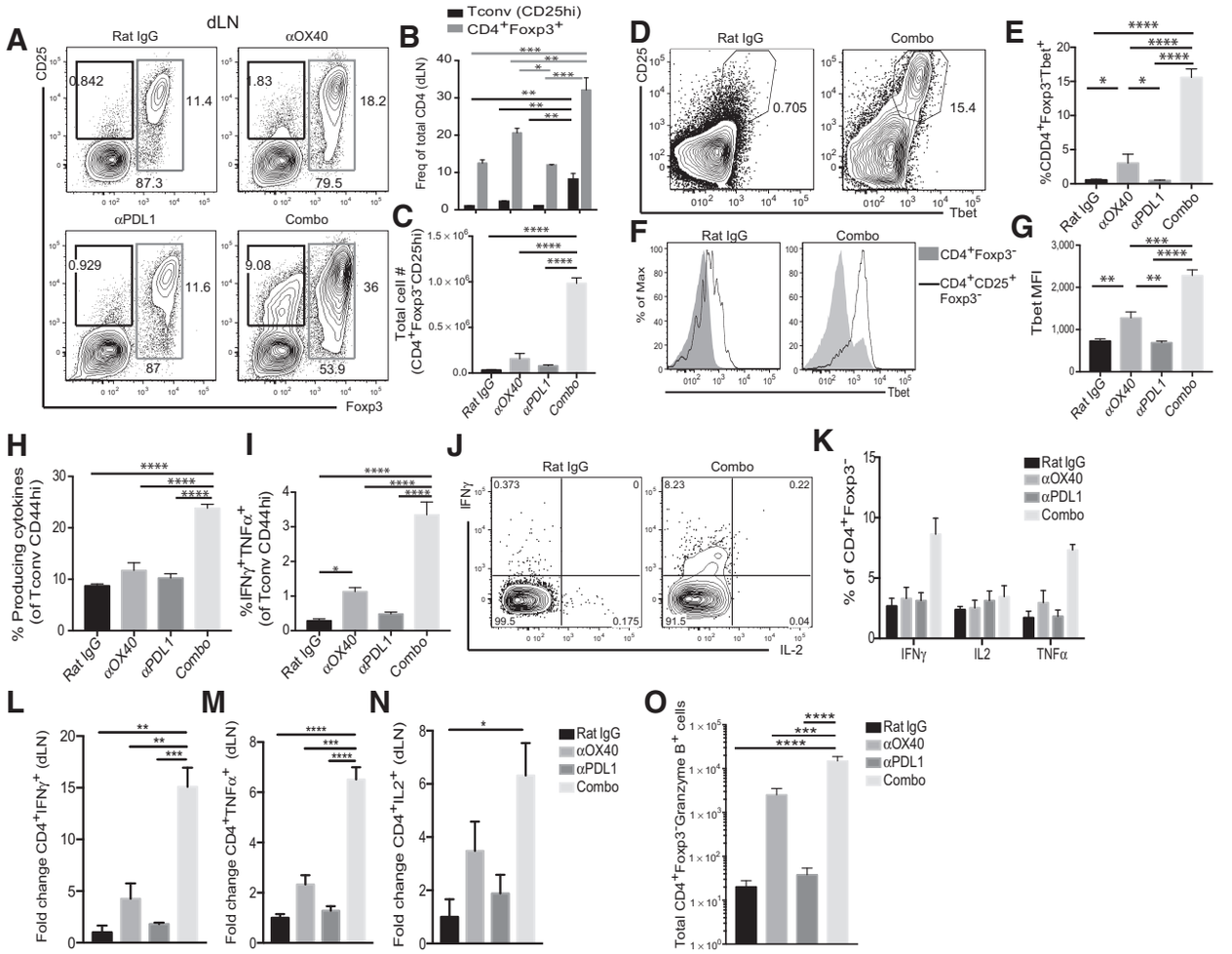

Figure 5.

Th1 skewed CD4$^+$ T-cell response after combination therapy. **A,** Representative flow cytogram and (**B**) tabulated frequency of CD4$^+$ T cells isolated from d42m1-T3 tumor–bearing mice 17 to 20 days after tumor inoculation and treatment. **C,** Changes in the total number of CD4$^+$CD25$^+$Foxp3$^-$ (Tconv). Flow-cytometric data of (**D**) Tbet expression and (**E**) tabulated frequencies of Tconv Tbet$^+$ CD4 T cells. **F,** Histogram overlays (CD4$^+$Foxp3$^-$CD25hi, solid black line; and total CD4$^+$Foxp3$^-$, shaded histogram) (**G**) and tabulated MFI in CD25hi CD4$^+$ T cells in the tumor-draining lymph nodes. **H,** Frequency of tumor-infiltrating CD4$^+$Foxp3$^-$ T cells making any cytokine after stimulation, (**I**) frequency of CD4$^+$IFNγ$^+$TNFα within the tumor, (**J**) representative cytogram of cytokine expression of digested tumor preparations stimulated with PMA/ionomycin and (**K**) tabulated expression of each individual cytokine. Fold change over rat IgG in (**L**) IFNγ, (**M**) TNFα, or (**N**) IL2 in the tumor dLNs after PMA/ionomycin or anti-CD3 stimulation. **O,** Total number of CD4$^+$Foxp3$^-$GzmB$^+$ T cells in the tumor. Data are representative of 3 or more experiments with 3 animals per treatment group per experimental replicate. One-way ANOVA was used for multiple comparison statistical analysis; SEM graphed. *, $P < 0.05$; **, $P < 0.01$; ***, $P < 0.001$; ****, $P < 0.0001$.

dissected further, we observed an increase in IFNγ- and TNFα-producing CD4$^+$Foxp3$^-$ T cells (Fig. 5J and K), TILs with a minimal effect of the combination therapy on the frequency of IL2-producing cells (Fig. 5J and K). Combination therapy significantly increased the frequency of Tconv in the tumor dLNs producing IFNγ (Fig. 5L), TNFα (Fig. 5M), and IL2 (Fig. 5N), an observation that supports the expansion of T cells in this tissue (Fig. 2D). Moreover, there was a 3-fold increase over the control in the total number of granzyme B+ Tconv after OX40 agonist immunotherapy alone, and this was modestly increased with PD-L1 blockade combination therapy (Fig. 5O). PD-L1 blockade had no effect on total granzyme B production compared with the control antibody. These data suggest that combination immunotherapy enhances Th1 differentiation of Tconv.

Combination therapy differentiates Tregs to an effector phenotype within the tumor

Because we observed a significant increase in the frequency of CD4$^+$Foxp3$^+$ and Foxp3$^-$ T cells in the lymph node after combination therapy (Fig. 5A), we evaluated proliferation. There was a 4-fold increase over control in Treg proliferation (defined as Ki67$^+$) in the tumor dLNs and spleen and a 2-fold increase in Tconv CD4$^+$ T cells (Fig. 6A–C). The ratio of Tconv and effector CD8$^+$ T cells to Tregs within the tumor can be a biomarker for therapeutic outcome (18). Within the tumor, Tconv had a greater proliferative capacity than Tregs by 1.5-fold after combination therapy, an observation that was unique to combination therapy–treated animals and restricted to the tumor microenvironment (Fig. 6D and E). The ratio of proliferating CD8$^+$ T cells to Tregs

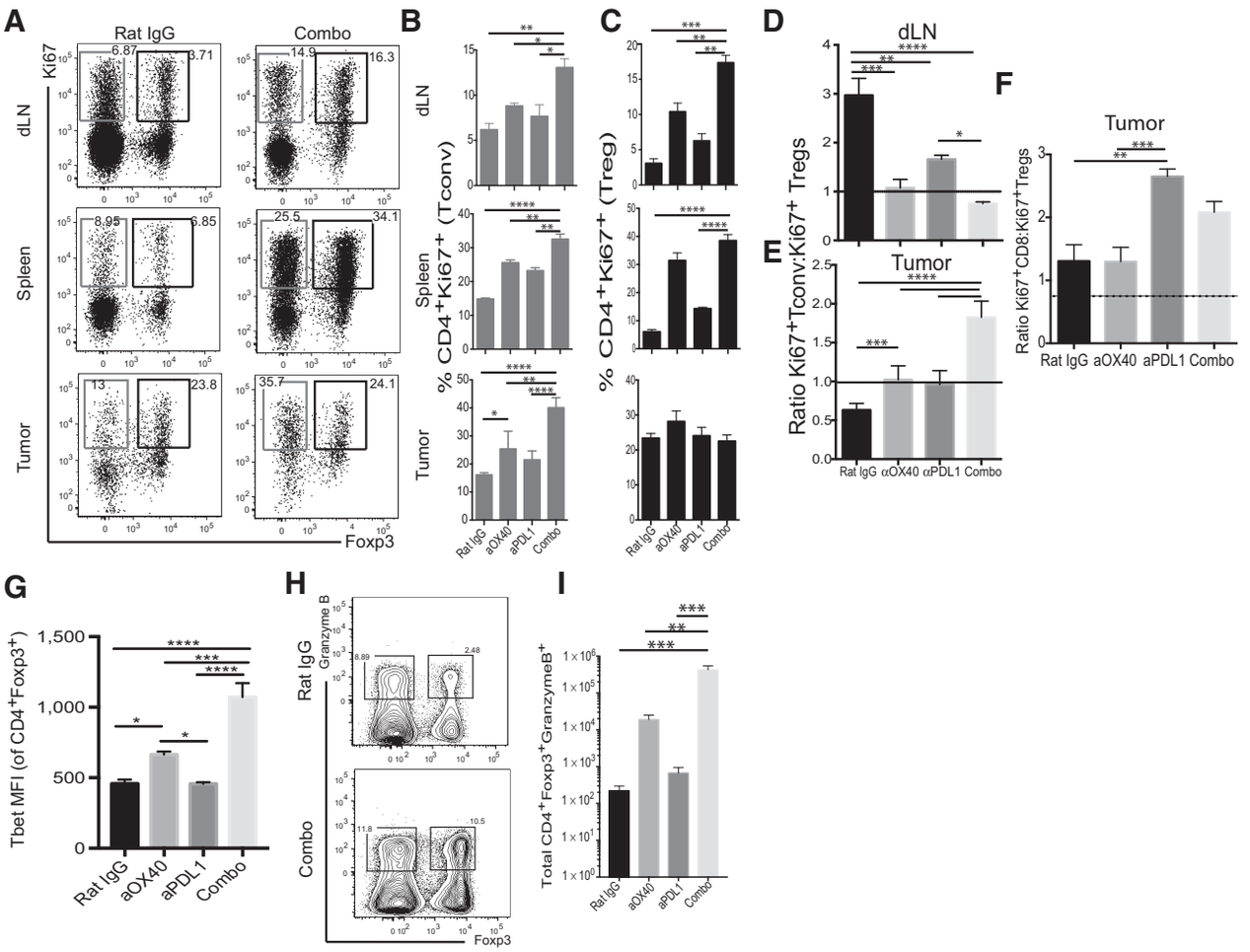

Figure 6.

Tregs gain effector function within the tumor. **A,** Representative flow cytogram and (**B–C**) tabulated data of Ki67$^+$CD4$^+$ T cells from tumor dLNs, spleen, and tumor of d42m1-T3 tumor–bearing animals. Ratio of Ki67$^+$CD4 Tconv in the (**D**) tumor dLNs and (**E**) tumor. **F,** Ratio of effector CD8$^+$ T cells to proliferating Tregs in the tumor. **G,** Tbet MFI of CD4$^+$Foxp3$^+$ T cells isolated from the tumor. **H,** Representative flow cytogram and (**I**) total number of CD4$^+$Foxp3$^+$ T cells making granzyme B directly *ex vivo* from the tumor. Data are representative of 2 or more experiments with at least 2–3 animals per group per experiment. One-way ANOVA was used for statistical analysis. *, $P < 0.05$; **, $P < 0.01$; ***, $P < 0.001$; ****, $P < 0.0001$.

within the tumor was also favorable, a change driven by PD-L1 blockade (Fig. 6F). This suggested that although combination therapy boosts the proliferation of Tregs, within the tumor, there is an enhanced ratio of effector cells to Tregs.

Given the strong Th1 skewing of the Tconv response (Fig. 5L–N), we explored if the Tregs within this environment mirrored this phenotypic lineage. We observed an increase in Tbet expression within the Treg compartment in the tumor after combination therapy (Fig. 6G). OX40 agonists slightly increased this skewing (Fig. 5E), but the combination treatment more than doubled the Tbet MFI within the CD4$^+$Foxp3$^+$ T cells. Given this observation and the increase in granzyme B production by CD4$^+$ Tconv cells, we also evaluated the production of granzyme B in Tregs. The frequency (Fig. 6H) and total number (Fig. 6I) of granzyme B–producing Tregs in the tumor after combination therapy increased as compared with the control group. Furthermore, these Tregs suppressed as well as Tregs from control-treated animals in an *ex vivo* suppression assay (Supplementary Fig. S4). Thus, combination therapy appears to promote the acquisition of effector function of a subset of Tregs within the tumor microenvironment.

Combination therapy enhances the metabolic function of antigen-specific T cells

OX40 agonists can increase the mRNA expression of a glucose transporter, Glut1, on T cells (4), and PD-L1 is reported to promote glucose uptake by tumor cells; therefore, we asked if immunotherapy modified the metabolic profile of antigen-specific CD8$^+$ T cells.

Uncertain we could isolate enough tumor-infiltrating T cells from control-treated animals, we addressed the metabolic potential of immunotherapy-treated T cells in an infection model in which we could isolate robust numbers of antigen-specific T cells (19). Mice were infected with *Listeria monocytogenes* (20) that expressed OVA and treated with single or combination therapy agents. At the peak of the antigen-specific response, we isolated

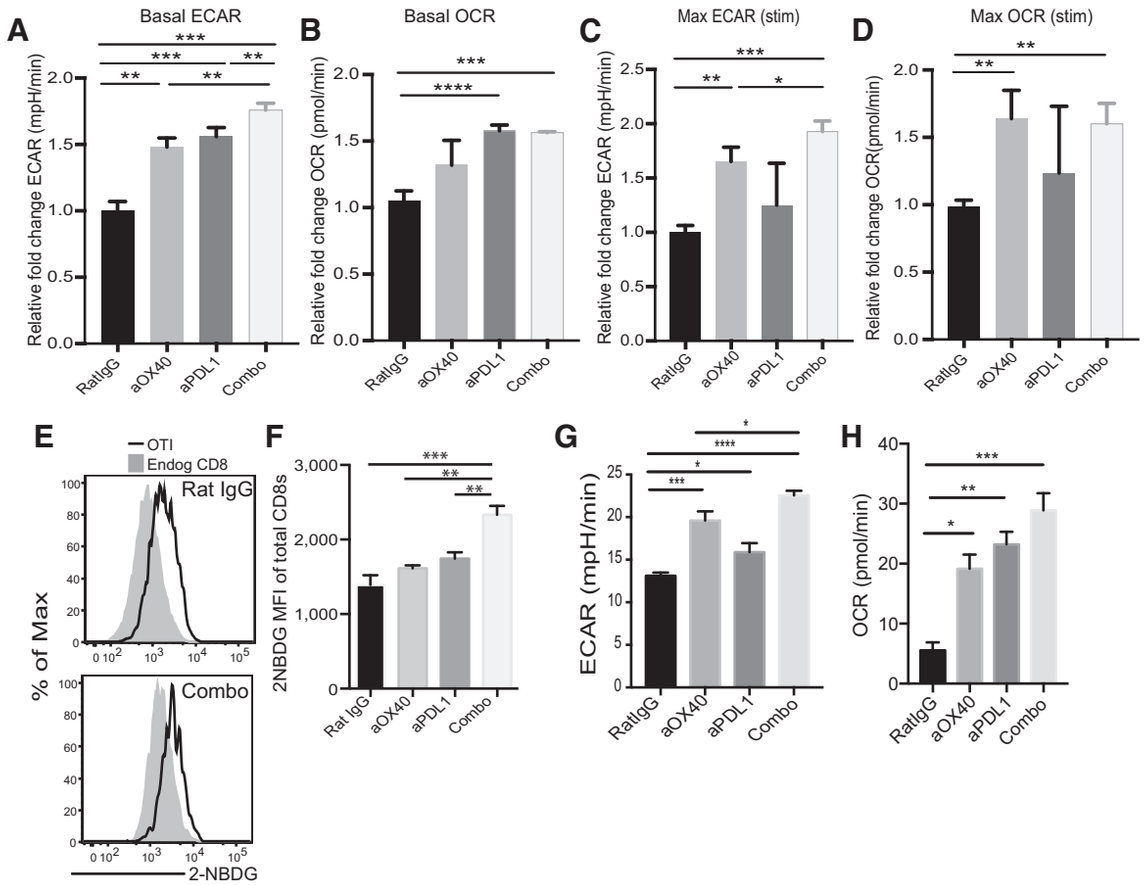

Figure 7.

Combination therapy drives a metabolic change in antigen-specific CD8$^+$ T cells. **A,** Basal extracellular acidification rate (ECAR, measure of aerobic glycolysis), and (**B**) OCR (measure of OXPHOS activity) and (**C**) Max ECAR and (**D**) OCR of ovalbumin-specific tetramer (SIINFEKL) + CD8$^+$ T cells isolated from *Listeria monocytogenes-ova*–infected animals. Measured by Seahorse XFe Analyzer; relative fold change is calculated based on the rat IgG-treated group at basal rates and at maximum activation (after PMA/ionomycin). TIL preparations were pulsed with 2NBDG; **E,** representative histogram and **F,** tabulated 2NBDG MFI from the tumor. OTI; Thy1.1 T cells were sorted from the tumor of MCA205-OVA–bearing animals and (**G**) aerobic glycolysis and (**H**) OXPHOS was measured by Seahorse. Data are representative of at least 2 independent experiments with more than 5 animals per treatment condition per experiment. *, $P < 0.05$; **, $P < 0.01$; ***, $P < 0.001$; *****, $P < 0.0001$.

OVA-specific CD8$^+$ T cells from the spleen of infected animals and measured their metabolic function using a Seahorse extracellular flux analyzer. All immunotherapy treatments increased the basal rate of glycolysis over the control-treated animals, and the most significant increase was following the combination therapy (Fig. 7A; Supplementary Fig. S5). Changes in glucose utilization and mitochondrial function may also be appreciated through changes in oxidative phosphorylation (OXPHOS) within the cell and we also observed that T cells from the treated groups had an increase in OXPHOS (Fig. 7B; Supplementary Fig. S5) compared with the rat IgG control.

Tumor-infiltrating lymphocytes are speculated to continuously encounter antigen, and persistent TCR triggering is metabolically demanding (21). Therefore, we tested the hypothesis that immunotherapy-treated T cells might have a different ability to metabolically respond to TCR ligation when compared with untreated T cells. We stimulated antigen-specific CD8$^+$ T cells from infected animals with PMA/ionomycin and measured their bioenergetic response in real time (22). Immunotherapy increased glycolysis (maximum ECAR; Fig. 7C) and OXPHOS (OCR; Fig. 7D) of antigen-specific CD8$^+$ T cells upon T-cell activation a finding consistent with previous work (9).

Extending our studies to the tumor microenvironment, we implanted OVA-tolerant mice (POET; ref. 23) with MCA205-OVA tumors and adoptively transferred congenically distinct OVA-specific CD8$^+$ T cells (OTI). Animals were treated similar to the treatment schedule depicted in Fig. 1A. Upon harvest of tumors, we pulsed tumor preparations *ex vivo* with a fluorescent glucose analogue, 2-(N-[7-nitrobenz-2-oxa-1,3-diazol-4-yl]amino)-2-deoxyglucose (2-NBDG), to discriminate cells by their functional ability to take up glucose and observed a significant increase in 2-NBDG uptake by tumor-infiltrating CD8$^+$ T cells (Fig. 7E and F) after combination therapy. Both the endogenous polyclonal and OTI T cells took up more 2NBDG as compared with the control, highlighting changes in the tumor microenvironment (Fig. 7E). Utilizing this adoptive transfer model, we sorted tumor antigen–specific OTI T cells and assessed their glycolytic potential. We observed a significant

increase in basal aerobic glycolysis (ECAR) of $CD8^+$ T cells after immunotherapy (Fig. 7G). Anti-OX40 increased ECAR, whereas PD-L1 blockade showed only a modest increase over the control group. The combination therapy also had a significant impact on $CD8^+$ T-cell OXPHOS (Fig. 7H). These data suggest that overall bioenergetic fitness of antigen-specific $CD8^+$ T cells is increased with anti-OX40 + anti–PD-L1 treatment, findings that support the enhanced T-cell–mediated antitumor responses reported.

Discussion

Inhibiting the PD-1/PD-L1 axis in late-stage cancers has achieved unprecedented success in tumor regression. Because this is a receptor–ligand pair, a common hypothesis is that targeting one, i.e., PD-1, will impart the same biological and clinical benefit as targeting the other, i.e., PD-L1. This simplistic view, however, overlooks the unique expression of each of these molecules within the tumor microenvironment and the distinct signaling pathways that may or may not be activated by blocking antibodies. In addition, it has been reported by multiple groups that PD-1 blockade and OX40 agonist combination therapy is deleterious to OX40 agonist therapy alone (10, 12), whereas another group published their synergy (24). In the deleterious studies, a reduction in tumor-infiltrating T cells was reported highlighting the importance of designing combination therapy approaches that do not deplete antigen-specific T cells. It is appreciated that some IgG isotypes bind to Fcγ receptors with very high-affinity and mediate antibody-dependent cellular cytotoxicity (ADCC). However, in preclinical immunotherapy studies, *in vivo* antibodies can be from different species with varying IgG affinities for Fcγ receptors and unknown ADCC potential. Some of the differences in our studies and those previously reported by others (10, 12) could be explained in part by the use of different anti–PD-1 clones and/or the biology of targeting PD-1 versus PD-L1. This article highlights a mechanism of action of targeting T-cell–intrinsic and –extrinsic pathways that enhances T-cell metabolic fitness, function, and antitumor immunity. Ultimately, this study could be used as a scientific road map to understand how these agents positively affect T-cell function in cancer patients.

Tumor antigen–specific T cells are regulated by both costimulatory and coinhibitory signals in the tumor microenvironment. Successful clinical approaches in cancer immunotherapy help restore the function of unresponsive T cells by blocking inhibitory pathways known as checkpoint blockade (25, 26). We and others have shown that providing exogenous costimulatory signals to T cells (e.g., OX40, 4-1BB, ICOS, or GITR agonists; refs. 27–31) also enhances antitumor immunity and hence provides a rationale for combination therapy with checkpoint blockade. Moreover, OX40 agonists have been shown to increase the therapeutic effects of CTLA-4 and PD-1 blockade (24, 32) in tumor-bearing mice, and currently both of these combination approaches are in the clinic without a clear mechanism of synergy or biomarkers of response.

In addition to enhanced $CD8^+$ T-cell responses, we also report an increase in $CD4^+$ T-cell differentiation and function of Th1 and Treg cells in combination therapy–treated animals. Despite an increase in Treg frequency in the periphery, within the tumor the combination therapy enhanced the expression of the Th1 transcription factor Tbet in a subset of Tregs, and ∼10% of the $CD4^+Foxp3^+$ TIL expressed the protease granzyme B at the time of harvest. The acquisition of effector function by a subset of Tregs is observed in the tumor microenvironment, where we observe robust antitumor T-cell responses. Consistent with this observation is evidence that the stability and function of Tregs is compromised within some tumors via the acquisition of IFNγ production by $Foxp3^+$ Tregs. Overacre-Delgoffe and colleagues illustrate a feed-forward loop between IFNγ signaling and Treg fragility, a phenotype that is restricted to the tumor microenvironment and associated with robust antitumor immunity (33). Rudensky's laboratory reported on the stability and function of $Tbet^+$ Tregs, and in RNA-seq analysis of $Tbet^+$ and $Tbet^-$ $Foxp3^+$ cells, they observe a significant increase in granzyme B expression in $Tbet^+$ Tregs (34). Although Rudensky and colleagues ultimately hypothesize that $Tbet^+$ Tregs directly suppress Th1 and $CD8^+$ T cells, the data presented fell short in evaluating the effector function of $Tbet^+Foxp3^+$ T cells, the cell subset expanded herein with combination therapy. Rather, the authors evaluated the function of $CD4^+Foxp3^-$ cells. Here, we observed robust proliferation of conventional $CD4^+$ and $CD8^+$ T cells in the presence of $Tbet^+Foxp3^+$ T cells derived from the tumor microenvironment. And we observed no difference in the ability of these Tregs to suppress T-cell proliferation in a classic Treg suppression assay.

Despite robust increase in Th1 T cells after combination therapy, the depletion of $CD4^+$ T cells did not affect the overall survival. This observation is difficult to interpret given the depletion of both Tconv and Tregs, only a subset of which gained effector function. Thus, the data suggest that the increase in Th1 differentiated effector T cells could in part support the expansion and plasticity of a subset of Tregs while simultaneously enhancing the functionality of $CD8^+$ T cells, which ultimately mediate increased tumor destruction.

Effector function is a metabolically demanding process (19), and nutrient availability influences effector cytokine production (35). Thus, it is plausible that altering cellular metabolism can influence the outcome of a T-cell response. PD-1, PD-L1, or CTLA-4 blockade therapy can partially restore these metabolic defects in tumor-infiltrating T cells (9); therefore, this may be a shared mechanism of action of these agents. Anti-OX40 therapy increases expression of Glut1 and hexokinase-2 (4), suggesting a direct effect of OX40 receptor ligation on the metabolic potential of $CD4^+$ T cells. In fact, our studies reveal a consequence of OX40 receptor ligation on metabolic function in the context of both infection and cancer. Considering our $CD8^+$ T-cell functional data, it is intriguing to postulate that the increase in effector function is supported by an increase in glucose uptake and more efficient cellular respiration, as was shown by Chang and colleagues (9).

In conclusion, concurrent PD-L1 blockade with an OX40 agonist enhanced $CD4^+$ and $CD8^+$ T-cell function, promoted the acquisition of effector molecules by a subset of Tregs and increased late-stage tumor destruction, enhancing long-term disease-free survival. Human clinical trials are assessing whether this combination leads to increased cytokine and cytolytic capacity in cancer patients (NCT02705482). This study highlights possible biomarkers and emphasizes the importance of interrogating multiple parameters of immune cell function in these clinical samples. Together, these preclinical observations may help define changes that occur in patients who ultimately derive clinical benefit from this combination immunotherapy.

Disclosure of Potential Conflicts of Interest

A. Weinberg is President/CSO of, has received commercial research funding from, and has ownership interest in AgonOx. No potential conflicts of interest were disclosed by the other authors.

Authors' Contributions

Conception and design: A.D. Weinberg, A.E. Moran
Development of methodology: F. Polesso, A.E. Moran
Acquisition of data (provided animals, acquired and managed patients, provided facilities, etc.): F. Polesso, A.E. Moran
Analysis and interpretation of data (e.g., statistical analysis, biostatistics, computational analysis): F. Polesso, A.D. Weinberg, A.E. Moran
Writing, review, and/or revision of the manuscript: F. Polesso, A.D. Weinberg, A.E. Moran
Administrative, technical, or material support (i.e., reporting or organizing data, constructing databases): F. Polesso, A.E. Moran
Study supervision: A.D. Weinberg, A.E. Moran

Acknowledgments

We are grateful to the NIH Tetramer Core for generating tetramers used for studies presented in this article. This work is supported in part by an American Cancer Society postdoctoral fellow grant PF-14-053-01 and an NIH grant T32AI078903 to A.E. Moran. A.D. Weinberg was funded by an NIH 5R01CA102577 grant, a sponsored research agreement with MedImmune, and the Providence Medical Foundation.

The costs of publication of this article were defrayed in part by the payment of page charges. This article must therefore be hereby marked *advertisement* in accordance with 18 U.S.C. Section 1734 solely to indicate this fact.

Received April 6, 2018; revised August 13, 2018; accepted December 14, 2018; published first December 18, 2018.

References

1. Moran AE, Polesso F, Weinberg AD. Immunotherapy expands and maintains the function of high-affinity tumor-infiltrating CD8 T cells in situ. J Immunol 2016;197:2509–21.
2. Moran AE, Kovacsovics-Bankowski M, Weinberg AD. The TNFRs OX40, 4-1BB, and CD40 as targets for cancer immunotherapy. Curr Opin Immunol 2013;25:230–7.
3. Redmond WL, Triplett T, Floyd K, Weinberg AD. Dual anti-OX40/IL-2 therapy augments tumor immunotherapy via IL-2R-mediated regulation of OX40 expression. PLoS One 2012;7:e34467.
4. Huddleston CA, Weinberg AD, Parker DC. OX40 (CD134) engagement drives differentiation of CD4+ T cells to effector cells. Eur J Immunol 2006;36:1093–103.
5. Vogel KU, Edelmann SL, Jeltsch KM, Bertossi A, Heger K, Heinz GA, et al. Roquin paralogs 1 and 2 redundantly repress the Icos and Ox40 costimulator mRNAs and control follicular helper T cell differentiation. Immunity 2013;38:655–68.
6. Yamazaki T, Akiba H, Iwai H, Matsuda H, Aoki M, Tanno Y, et al. Expression of programmed death 1 ligands by murine T cells and APC. J Immunol 2002;169:5538–45.
7. Keir ME, Butte MJ, Freeman GJ, Sharpe AH. PD-1 and its ligands in tolerance and immunity. Annu Rev Immunol 2008;26:677–704.
8. Hui E, Cheung J, Zhu J, Su X, Taylor MJ, Wallweber HA, et al. T cell costimulatory receptor CD28 is a primary target for PD-1-mediated inhibition. Science 2017;355:1428–33.
9. Chang CH, Qiu J, O'Sullivan D, Buck MD, Noguchi T, Curtis JD, et al. Metabolic competition in the tumor microenvironment is a driver of cancer progression. Cell 2015;162:1229–41.
10. Shrimali RK, Ahmad S, Verma V, Zeng P, Ananth S, Gaur P, et al. Concurrent PD-1 blockade negates the effects of OX40 agonist antibody in combination immunotherapy through inducing T-cell apoptosis. Cancer Immunol Res 2017;5:755–66.
11. Bonavita E, Gentile S, Rubino M, Maina V, Papait R, Kunderfranco P, et al. PTX3 is an extrinsic oncosuppressor regulating complement-dependent inflammation in cancer. Cell 2015;160:700–14.
12. Messenheimer DJ, Jensen SM, Afentoulis ME, Wegmann KW, Feng Z, Friedman DJ, et al. Timing of PD-1 blockade is critical to effective combination immunotherapy with anti-OX40. Clin Cancer Res 2017;23:6165–77.
13. Wu D, Sherwood A, Fromm JR, Winter SS, Dunsmore KP, Loh ML, et al. High-throughput sequencing detects minimal residual disease in acute T lymphoblastic leukemia. Sci Transl Med 2012;4:134ra63.
14. Adurthi S, Kumar MM, Vinodkumar HS, Mukherjee G, Krishnamurthy H, Acharya KK, et al. Oestrogen Receptor-alpha binds the FOXP3 promoter and modulates regulatory T-cell function in human cervical cancer. Sci Rep 2017;7:17289.
15. Currie AJ, Prosser A, McDonnell A, Cleaver AL, Robinson BW, Freeman GJ, et al. Dual control of antitumor CD8 T cells through the programmed death-1/programmed death-ligand 1 pathway and immunosuppressive CD4 T cells: regulation and counterregulation. J Immunol 2009;183:7898–908.
16. Moran AE, Holzapfel KL, Xing Y, Cunningham NR, Maltzman JS, Punt J, et al. T cell receptor signal strength in Treg and iNKT cell development demonstrated by a novel fluorescent reporter mouse. J Exp Med 2011;208:1279–89.
17. Gunderson AJ, Kaneda MM, Tsujikawa T, Nguyen AV, Affara NI, Ruffell B, et al. Bruton tyrosine kinase-dependent immune cell cross-talk drives pancreas cancer. Cancer Discov 2016;6:270–85.
18. Onizuka S, Tawara I, Shimizu J, Sakaguchi S, Fujita T, Nakayama E. Tumor rejection by in vivo administration of anti-CD25 (interleukin-2 receptor alpha) monoclonal antibody. Cancer Res 1999;59:3128–33.
19. Pearce EL, Poffenberger MC, Chang CH, Jones RG. Fueling immunity: insights into metabolism and lymphocyte function. Science 2013;342:1242454.
20. Glodde N, Bald T, van den Boorn-Konijnenberg D, Nakamura K, O'Donnell JS, Szczepanski S, et al. Reactive neutrophil responses dependent on the receptor tyrosine kinase c-MET limit cancer immunotherapy. Immunity 2017;47:789–802e9.
21. Scharping NE, Menk AV, Moreci RS, Whetstone RD, Dadey RE, Watkins SC, et al. The tumor microenvironment represses T cell mitochondrial biogenesis to drive intratumoral T cell metabolic insufficiency and dysfunction. Immunity 2016;45:701–3.
22. van der Windt GJ, O'Sullivan D, Everts B, Huang SC, Buck MD, Curtis JD, et al. CD8 memory T cells have a bioenergetic advantage that underlies their rapid recall ability. Proc Natl Acad Sci USA 2013;110:14336–41.
23. Lees JR, Charbonneau B, Swanson AK, Jensen R, Zhang J, Matusik R, et al. Deletion is neither sufficient nor necessary for the induction of peripheral tolerance in mature CD8+ T cells. Immunology 2006;117:248–61.
24. Guo Z, Wang X, Cheng D, Xia Z, Luan M, Zhang S. PD-1 blockade and OX40 triggering synergistically protects against tumor growth in a murine model of ovarian cancer. PLoS One 2014;9:e89350.
25. Hodi FS, O'Day SJ, McDermott DF, Weber RW, Sosman JA, Haanen JB, et al. Improved survival with ipilimumab in patients with metastatic melanoma. N Engl J Med 2010;363:711–23.
26. Topalian SL, Hodi FS, Brahmer JR, Gettinger SN, Smith DC, McDermott DF, et al. Safety, activity, and immune correlates of anti–PD-1 antibody in cancer. N Engl J Med 2012;366:2443–54.
27. Fan X, Quezada SA, Sepulveda MA, Sharma P, Allison JP. Engagement of the ICOS pathway markedly enhances efficacy of CTLA-4 blockade in cancer immunotherapy. J Exp Med 2014;211:715–25.
28. Melero I, Shuford WW, Newby SA, Aruffo A, Ledbetter JA, Hellstrom KE, et al. Monoclonal antibodies against the 4-1BB T-cell activation molecule eradicate established tumors. Nat Med 1997;3:682–5.

29. Weinberg AD, Rivera MM, Prell R, Morris A, Ramstad T, Vetto JT, et al. Engagement of the OX-40 receptor in vivo enhances antitumor immunity. J Immunol 2000;164:2160–9.
30. Ko K, Yamazaki S, Nakamura K, Nishioka T, Hirota K, Yamaguchi T, et al. Treatment of advanced tumors with agonistic anti-GITR mAb and its effects on tumor-infiltrating Foxp3+CD25+CD4+ regulatory T cells. J Exp Med 2005;202:885–91.
31. Turk MJ, Guevara-Patino JA, Rizzuto GA, Engelhorn ME, Sakaguchi S, Houghton AN. Concomitant tumor immunity to a poorly immunogenic melanoma is prevented by regulatory T cells. J Exp Med 2004;200:771–82.
32. Redmond WL, Linch SN, Kasiewicz MJ. Combined targeting of costimulatory (OX40) and coinhibitory (CTLA-4) pathways elicits potent effector T cells capable of driving robust antitumor immunity. Cancer Immunol Res 2014;2:142–53.
33. Overacre-Delgoffe AE, Chikina M, Dadey RE, Yano H, Brunazzi EA, Shayan G, et al. Interferon-gamma drives T_{reg} fragility to promote antitumor immunity. Cell 2017;169: 1130–41e11.
34. Levine AG, Mendoza A, Hemmers S, Moltedo B, Niec RE, Schizas M, et al. Stability and function of regulatory T cells expressing the transcription factor T-bet. Nature 2017;546:421–5.
35. Chang CH, Curtis JD, Maggi LB Jr, Faubert B, Villarino AV, O'Sullivan D, et al. Posttranscriptional control of T cell effector function by aerobic glycolysis. Cell 2013;153:1239–51.